Radiative Properties and Excitons of Candidate Defect Emitters in Hexagonal Boron Nitride

Shiyuan Gao, Hsiao-Yi Chen, and Marco Bernardi*

Department of Applied Physics and Material Science, California Institute of Technology, Pasadena, California 91125, USA

E-mail: bmarco@caltech.edu

Abstract

Point defects in hexagonal boron nitride (hBN) have attracted growing attention as bright single-photon emitters. However, understanding of their atomic structure and radiative properties remains incomplete. Here we employ first-principles calculations to compute the structure, excited states and radiative lifetimes of over 20 native defects and carbon or oxygen impurities in hBN, generating a large data set of light emission energy, polarization and lifetime. Bayesian analysis of our results combined with existing experimental data allows us to identify the native $V_N N_B$ defect as the most likely single-photon emitter in hBN. Our work advances the microscopic understanding of hBN single-photon emitters and introduces a computational framework to systematically investigate defect emitters in 2D materials.

1

Two-dimensional (2D) materials are rapidly becoming a new platform for photon based quantum information technologies.[1,2] The discovery of single-photon emitters (SPEs) at point defects in hBN[3] has spurred an intense search for optically active defects in 2D crystals.[4] Compared to defects in bulk crystals such as diamond and silicon carbide,[5–8] defects embedded in 2D materials promise to be more easily addressed and controlled. In the case of hBN, defect emitters exhibit a range of desirable properties, including high emission rate, room temperature stability, strong zero-phonon line (ZPL) and easy integration with other optical components using 2D hBN crystals.[1,9–12]

A pressing challenge for defect emitters in hBN is identifying their atomic structure. Various possible structures have been proposed on the basis of density functional theory (DFT) calculations and their comparison with experiments.[3,13–19] However, while DFT can provide valuable insight into the formation energy, symmetry and electronic structure of SPE defects, it cannot address key aspects of point-defect SPEs such as their excited states and radiative processes responsible for light emission. To complicate the matter further, similar to other 2D materials and their defects,[20–22] optical transitions at defects in hBN are dominated by excitonic effects,[23] which require specialized first-principles calculations beyond the scope of DFT.

The Bethe-Salpeter equation (BSE) can accurately predict optical properties and excitons in materials.[24] It also enables, due to recent advances, precise calculations of radiative lifetimes in 2D and bulk crystals.[25–28] The radiative lifetime plays an important role in the study of SPEs as it determines the shortest decay time constant in the second-order photon correlation function[29,30] and can also be measured directly from fluorescence intensity decay.[3,10] Applying the BSE and related methods to defect emitters in hBN would enable direct comparisons between theory and experiment of the emission energy and radiative lifetime, providing valuable information to identify defect SPEs. Yet, first-principles BSE calculations are computationally costly to carry out on defect structures, and the radiative lifetime calculations are only a recent development.

In this work, we employ the BSE approach to compute from first principles the optical properties, transition dipoles, excitons and radiative lifetimes of atomic defects in hBN. We examine a large pool of candidate SPE structures, spanning native defects and carbon or oxygen impurities, and quantify their likelihood on the basis of their photophysics. Bayesian statistical analysis is employed to correlate our results with experiments and identify the most likely SPE defect structures in hBN, among which the $V_N N_B$ defect has the highest likelihood. In-depth calculations on the $V_N N_B$ defect highlight the strong dependence of its radiative properties on the atomic structure and dielectric screening. Our systematic investigation addresses key challenges for characterizing the excited states and radiative properties of defect emitters in 2D materials.

The ground state defect properties are computed using DFT with the QUANTUM ESPRESSO code,[31] employing fully relaxed defect atomic structures in 5×5 supercells of monolayer hBN (and for some defects, in bulk hBN). We then refine the electronic structure of selected defects using GW calculations,[32] followed by BSE calculations to obtain the exciton energies and wave functions and from them the optical absorption, transition dipoles and radiative lifetimes (see Methods). Our candidate structures consist of charge-neutral native defects and carbon or oxygen impurities occupying one or two atomic sites, for a total of 8 different native defects and 7 structures for each of carbon and oxygen impurities. In the following, we denote the defects in hBN as $X_N Y_B$ if neighboring N and B atoms are replaced by species X and Y, respectively, where X and Y can be a vacancy or another element.[3,13] We focus on emitters in the interior of the 2D crystal[33,34] and do not consider defects that would likely appear at the sample edges or corners.[35,36]

The electronic energies obtained using DFT, while in general not representative of electronic or optical transitions, can be used for guidance and for estimating qualitative trends. Figure 1 shows the lowest spin-conserving transition energy of the candidate defects, obtained from DFT, together with the emission polarization inferred from structural symmetry. The defect structures considered here exhibit three different local symmetries, D_{3h}, C_{2v}, and C_s.
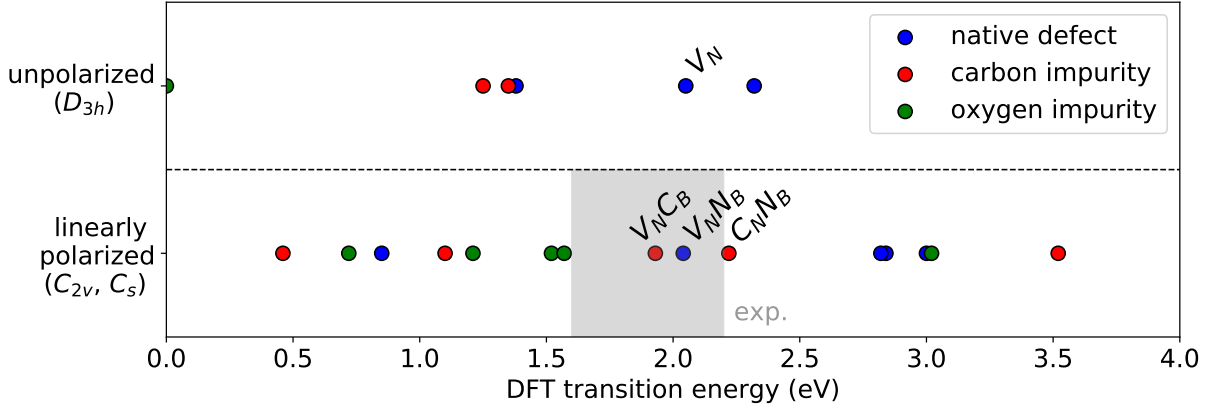
Figure 1. Distribution of the DFT transition energy, structural symmetry and emitted light polarization of 22 candidate defect structures. The shaded area shows the experimental range of values for SPEs in hBN.

In the high symmetry D_{3h} structure, adopted by N_B, V_N, B_N, C_B, C_N, O_N, emitted light cannot be linearly polarized. Conversely, linearly polarized emitted light, as observed experimentally in hBN SPEs,[11] is possible in the C_{2v} and C_s symmetries. In the C_{2v} configuration, which is the most common among the defects investigated here, the 3-fold rotational symmetry is broken but all the atoms remain in-plane, preserving the mirror symmetry with respect to the crystal plane. The C_s symmetry found in the $V_N N_B$, $V_N C_B$, $V_N O_B$ and O_B defects is instead associated with an out-of-plane distortion that breaks the mirror symmetry about the plane. The DFT transition energies for the 22 defect structures range from 0 to 3.5 eV. In contrast, the ZPL of the measured SPEs are in the $1.6-2.2$ eV energy range,[11] as shown by the shaded region in Fig. 1. While candidate structures with D_{3h} symmetry can be ruled out, C_{2v} and C_s structures with exceedingly small or large DFT transition energies also appear unlikely on the basis of the DFT results.

Starting from the DFT ground state, for selected defects we compute the excited state properties with the GW-BSE method, obtaining the quasiparticle energies in the one-shot G_0W_0 approximation and the exciton energies and wave functions with the ab initio BSE, which correctly captures electron-hole interaction and excitonic effects, using the Yambo code[37,38] (see Methods). Convergence tests with respect to supercell size are given in the
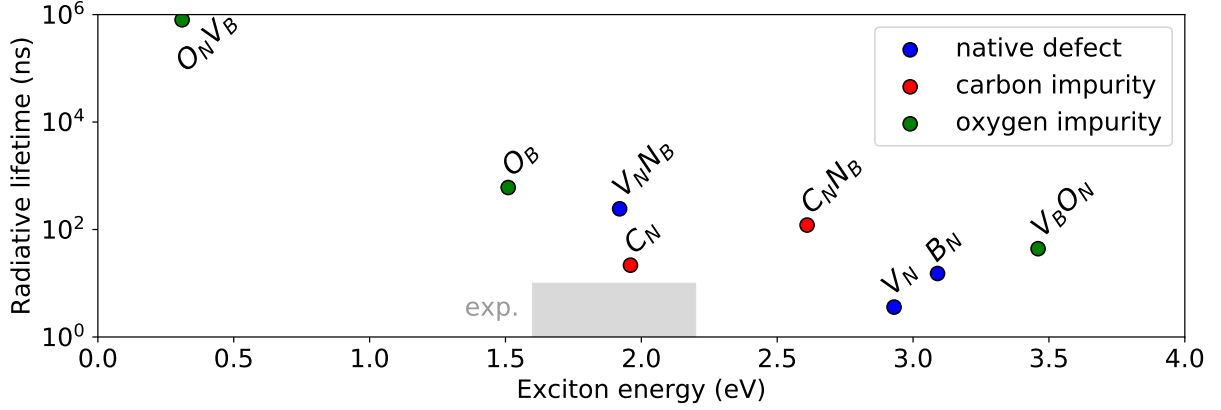
4

Figure 2. Radiative lifetime and energy of the lowest bright exciton of candidate defect SPEs in hBN from GW-BSE calculations. The range of experimental values is shown as a shaded region.

Supplementary Information. We combine the solutions of the BSE with an approach we recently developed [27,28] to compute the radiative lifetime of an exciton state, denoted by S, as the inverse of the decay rate γ_S obtained from Fermi's golden rule. Generalizing a formula we previously obtained for an isolated (0D) emitter, [27] as is appropriate for defect SPEs, we can account for anisotropic dielectric screening in hBN:

$$\gamma_S = \frac{\sqrt{\epsilon_{xy}}e^2 E_S}{3\pi\epsilon_0 m^2 c^3 \hbar^2} \left[\left(\frac{3}{4} + \frac{\epsilon_z}{4\epsilon_{xy}}\right) |p_{S,xy}|^2 + |p_{S,z}|^2 \right] , \tag{1}$$

where ϵ_{xy} and ϵ_z are the in-plane and out-of-plane dielectric constants of hBN, respectively, and $p_{S,xy}$ and $p_{S,z}$ are the corresponding components of the exciton transition dipole. Although our calculations for bulk hBN use a constant value of $\epsilon_{xy} = 5$, for monolayer hBN we account for the dependence of screening on the wavevector q by using $\epsilon_{xy}(q) \approx 1 + 2\pi\alpha_{2D} q$, [39] where α_{2D} is a constant equal to 0.4 nm. [40] In this approach, which is appropriate for 2D materials, the in-plane dielectric constant of monolayer hBN reduces to a unit value of 1 at optical frequencies.

Figure 2 shows the computed radiative lifetimes and lowest bright exciton energies for seven selected defects, including V_N, B_N, $V_N N_B$, C_N, $V_N C_B$, $O_N V_B$ and $V_B O_N$. We find that

5

the exciton energy can differ significantly − by as much as 1 eV − from the corresponding DFT transition energy, which fails to account for screening and electron-hole interaction effects. This result is a testament to the importance of excited state calculations for investigating SPEs. The computed radiative lifetime for the selected structures span six orders of magnitude, from about 1 to 10^6 ns, showing that the emission rate and brightness of defect emitters in hBN can vary widely. The values typically found in experiments for the emission energy (1.6−2.2 eV) and radiative lifetime (1−10 ns) are given for comparison in Fig. 2.

As the candidate defect structures have properties distributed across a wide range, it is challenging to pinpoint the correct defect structure from our results. As such, we pursue a quantitative analysis of the relative likelihood of the various structures using Bayesian inference, a statistical approach for dealing with uncertainties and combining information from different categories, in which the probability of a hypothesis is updated as more evidence or information becomes available.[41] The workflow of our analysis is shown in Fig. 3. We first generate candidate structures systematically by enumerating all defects that occupy no more than two adjacent atomic sites. Each candidate structure h is assigned a prior likelihood $p(h)$ on the basis of its structural complexity, using the single exponential form $p(h) \propto S_h A^{-C_h}$, where C_h measures the complexity of the structure, defined as the number of vacancies and antisite defects plus twice the number of impurities, A is a constant, and S_h is a degeneracy factor due to symmetry-related configurations. This prior likelihood is only an initial guess assumed without considering which defects could account for SPEs in hBN and derived using the intuitive fact that more complex point-defect structures are less likely to form. We subsequently combine our computational results with experimental evidence to obtain a posterior likelihood $p(h|E)$ for each structure:[41]

$$p(h|E) \propto p(h)p(E|h), \tag{2}$$

where the likelihood function $p(E|h)$ is the probability that the structure h is compatible with a specific piece of experimental evidence E on the basis of our calculations. The resulting

posterior likelihood, which is updated in multiple steps using several computed properties, quantifies which structures among those considered are more likely to be defect emitters in hBN and deserve further consideration.
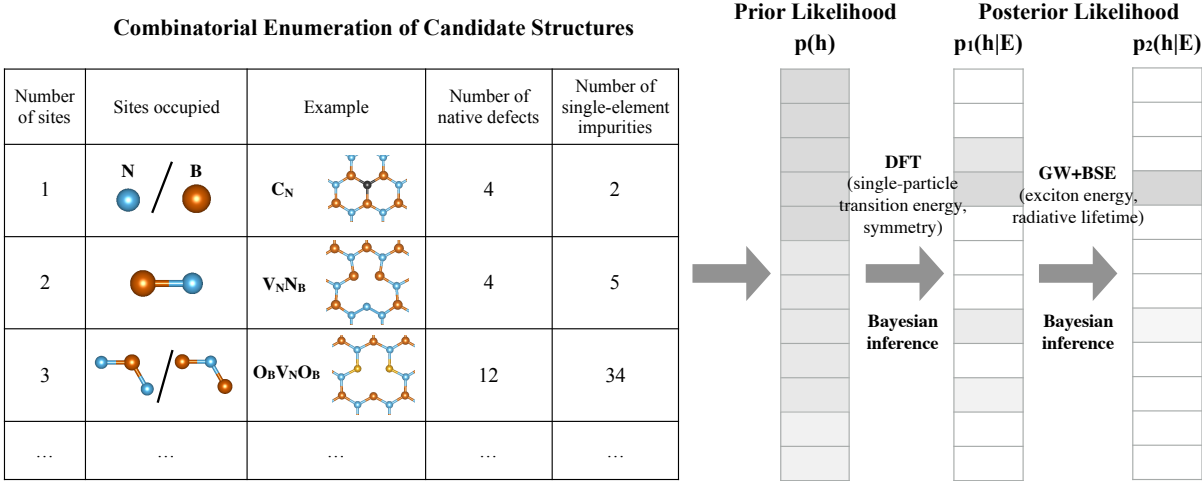

Figure 3. Bayesian inference workflow. Candidate structures are initially generated through combinatorial enumeration of point defects in hBN and attributed a prior likelihood based on structural complexity. The likelihood of each defect is then updated using results from our DFT calculations. For the most promising defect structures, the likelihood is refined using GW-BSE calculations.

The properties of the candidate SPE defects and the results of our Bayesian inference analysis are summarized in Table 1. Moving in the table from left to right, the prior probability $p(h)$ is updated to posterior probabilities $p(h|E)$ using calculations presented in subsequent columns. The first computed posterior probability, $p_1(h|E)$, uses the DFT results to infer whether the defect symmetry is compatible with linearly polarized emission and whether the DFT transition energy, within a standard deviation of $\sim$0.5 eV, falls in the $1.6-2.2$ eV emission range found in experiments.[10,11,33] The final posterior likelihood $p_2(h|E)$ in the rightmost column of Table 1 gives the likelihood of the most likely defect structures when all factors have been taken into account, including comparison between the lowest bright ex-

7

citon energy and the experimental emission energy and comparison with experiment of the radiative lifetime from our GW-BSE calculations. The detailed rationale of our Bayesian analysis is described in the Supplementary Information.

The main finding from the data in Table 1 is that the V_NN_B defect, which was originally proposed as a SPE in hBN on the basis of DFT calculations,[3,13,18] possesses optical and radiative properties that most accurately match the experimental results, even after taking into account excitonic effects and radiative lifetimes. The next most likely structure is the oxygen impurity defect, O_B, with an emission energy of 1.52 eV just below the experimental range. On the other hand, we find that the V_NC_B defect, which is also considered a likely candidate in the literature based on DFT calculations,[13,18] has an emission energy of 2.6 eV that lies too far above the experimental energy range when excitonic effects are included, making it a less likely candidate. As the most likely defect emitter in hBN is the V_NN_B structure according to our analysis, we investigate it in more detail to provide a microscopic understanding of its radiative properties.

Figure 4(a) shows that the relaxed atomic structure of the V_NN_B defect in monolayer hBN exhibits an out-of-plane displacement of the central nitrogen (N) atom by $z = 0.66$ Å. If the structure is made planar by constraining the N atom to the hBN plane, the total energy of the system is only moderately higher (by 0.125 eV) than the equilibrium structure. Therefore the total energy forms a shallow double-well potential as a function of the out-of-plane N atom displacement. Consistent with recent findings,[42] this small energy difference suggests that the structure is soft in the out-of-plane direction and could fluctuate due to external perturbations.

To take this result into account, we compute the optical absorption spectrum of the V_NN_B defect for out-of-plane displacements z of the N atom in the $0-0.83$ Å range, interpolating between the in-plane and out-of-plane equilibrium structures to obtain the intermediate metastable structures. We find that the absorption spectrum changes drastically for even small changes of z, as shown in Fig. 4(c). The spectrum is dominated by two exciton

type	defect	prior $p(h)$	polarized or not	energy (DFT, eV)	$p_1(h\|E)$ with DFT	energy (GW-BSE, eV)	rad. lifetime (GW-BSE, ns)	$p_2(h\|E)$ with GW-BSE
native defect	V_B	1	Y	0.66	0.19			
	N_B	1	N	2.32	<0.01			
	V_N	1	N	2.05	<0.01	2.93	3.6	<0.01
	B_N	1	N	2.20	<0.01	3.09	15	<0.01
	V_NV_B	0.26	Y	2.84	0.18			
	B_NV_B	0.26	Y	0.85	0.12			
	V_NN_B	0.26	Y	2.04	1	1.92	334	1
	B_NN_B	0.26	Y	2.82	0.2			
carbon impurity	C_B	0.26	N	1.35	<0.01			
	C_N	0.26	N	1.25	<0.01	1.96	21.7	<0.01
	C_NV_B	0.07	Y	1.15	0.09	1.02	1.7×10^5	<0.01
	C_NN_B	0.07	Y	2.22	0.22			
	V_NC_B	0.07	Y	1.93	0.27	2.61	121	0.01
	B_NC_B	0.07	Y	1.1	0.09			
	C_NC_B	0.02	Y	3.52	<0.01			
oxygen impurity	O_B	0.26	Y	1.51	0.79	1.52	605	0.38
	O_N	0.26	N	0	<0.01			
	O_NV_B	0.07	Y	0.72	0.02	0.31	1.7×10^6	<0.01
	O_NN_B	0.07	Y	1.57	0.22			
	V_NO_B	0.07	Y	3.02	0.02	3.46	44	<0.01
	B_NO_B	0.07	Y	1.21	0.11			
	O_NO_B	0.02	Y	3.41	<0.01			
experiments			Y		1.6 - 2.2		2 - 10	

Table 1. Calculated properties of candidate defect emitters in hBN and their likelihood based on Bayesian inference analysis. The likelihood is normalized to a maximum value of 1.

absorption peaks at low energy. At the equilibrium position ($z = 0.66$ Å), the first peak at 1.92 eV is associated with a transition from the top valence to the bottom conduction spin-majority electronic states, whose wave functions are shown in Fig. 4(b). As the displacement z of the N atom is decreased from the equilibrium value to zero, which corresponds to a planar structure, the energy of the first exciton peak decreases at first but then increases again at small z values while gaining oscillator strength monotonically. The second peak at 2.7 eV is also due to a transition from the top valence to the bottom conduction spin-minority bands with relatively large oscillator strength at the out-of-plane equilibrium N atom position. Both the energy and the oscillator strength of this peak decrease monotonically as z decreases [see Fig. 4(c)]. For the planar structure (z=0), the second peak becomes the lowest-energy transition but completely loses its oscillator strength and becomes a dark state.
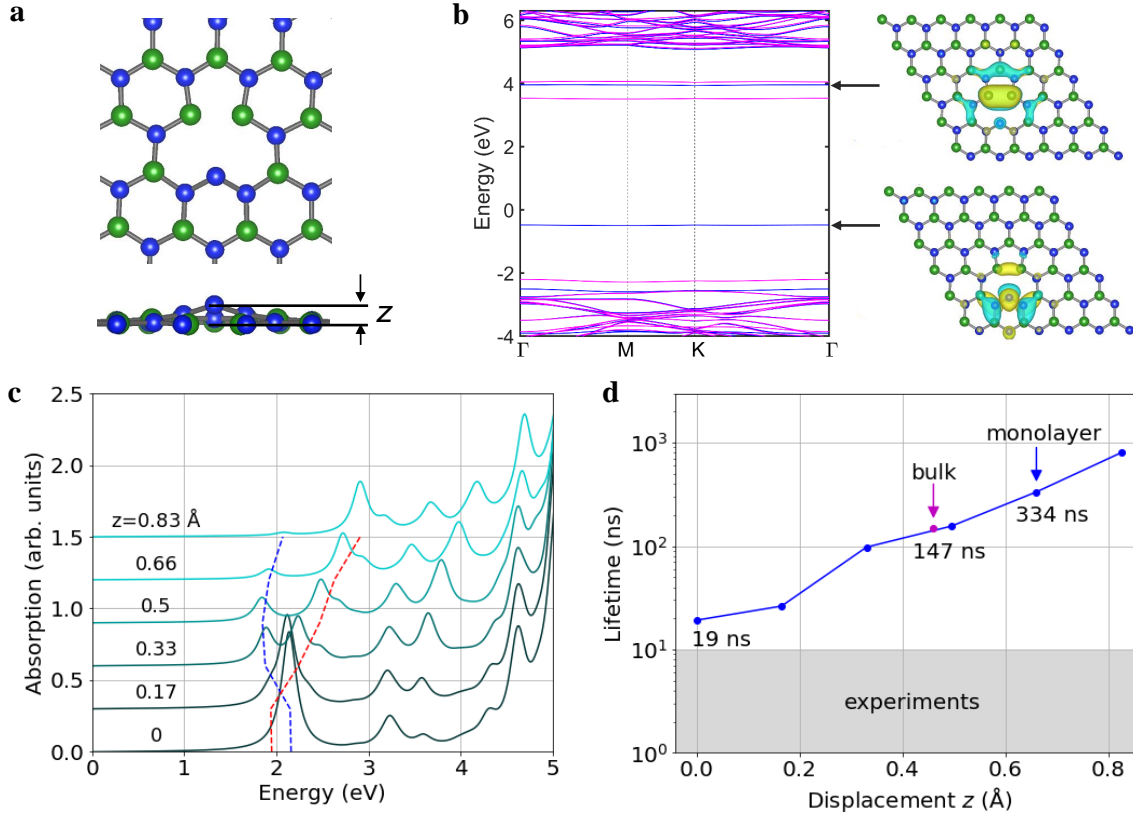
Figure 4. Properties of the $V_N N_B$ defect. (a) Atomic structure in top and side views, with N atoms shown as blue and B atoms as green spheres. Also shown in the side view is the N atom out-of-plane displacement z. (b) GW electronic band structure computed using a 5×5 supercell. The wave function of the two majority-spin bands that mainly contribute to the lowest-energy exciton are plotted on the right. (c) Absorption spectrum and (d) radiative lifetime as a function of the out-of-plane displacement z of the central N atom.

These noteworthy changes in the two lowest-energy exciton peaks are accompanied by substantial changes in the exciton radiative lifetimes. Although the lifetime of the lowest exciton is 334 ns for the DFT equilibrium out-of-plane distortion, it becomes only 19 ns if the $V_N N_B$ structure is kept planar ($z = 0$ case), as shown in Fig. 4(d). This value of the radiative lifetime for the planar structure is within a factor of $2-3$ of experimental results.[11] Because many experiments are carried out on thicker hBN samples, we also calculated the radiative lifetime of the $V_N N_B$ defect embedded in bulk hBN (instead of monolayer), a setting resembling more closely SPE experimental measurements in thicker hBN layer stacks (see Methods). Due to interlayer interactions, the out-of-plane displacement of the N atom is

10

reduced to 0.45 Å in bulk hBN. Going from monolayer to bulk reduces the radiative lifetime of the V_NN_B defect to 147 ns due to changes in the dielectric environment and transition dipole, both of which affect the radiative emission rate in Eq. (1). We conclude that the radiative lifetime is highly sensitive to both out-of-plane structural distortions and the dielectric environment.

While our computed lifetimes are in the $20-350$ ns range for different V_NN_B structures, these values pertain to an ideal defect with 100% quantum yield, whereas defect emission measured so far in hBN is likely associated with a lower quantum yield. To explain the discrepancy between the experimental and calculated lifetimes, note that nonradiative processes, which are not included in our calculation of intrinsic radiative lifetimes, could significantly reduce the apparent lifetime measured in experiments. For example, a defect with a measured 10 ns lifetime but only a 10% quantum yield would correspond to a 100 ns intrinsic radiative lifetime in very good agreement with our calculations. Future SPE measurements in hBN taking into account the quantum yield may provide a better estimate of the intrinsic SPE radiative lifetime and enable a more accurate comparison with our calculations.

In summary, we have investigated the excited state and radiative properties of many candidate defect SPEs in hBN. Our calculations address the photophysics of these defect structures, including their optical transitions and radiative lifetimes, using calculations that accurately account for excitonic effects and anisotropic dielectric screening. Our Bayesian statistical analysis allows us to identify the native V_NN_B defect as the most likely candidate within a wide pool of over 20 charge-neutral native defects and carbon or oxygen impurities. This work explores the fertile ground at the intersection of excited-state first-principles calculations and Bayesian learning methods, and the application of this framework to quantum technologies. The search for novel single emitters will greatly benefit from such precise first-principles calculations of excited states in materials.

Methods

We carry out DFT calculations in the generalized gradient approximation using the Perdew-Burke-Ernzerhof (PBE) exchange-correlation functional.[43] Our spin-polarized DFT calculations employ the plane-wave pseudopotential method implemented in QUANTUM ESPRESSO.[31] The defects are placed in a 5×5 supercell of hBN with a lattice constant kept fixed at 5×2.504 Å while the atoms are fully relaxed without symmetry constraints. For calculations on monolayer hBN, a vacuum of 15 Å is used to avoid spurious inter-layer interactions with the periodic replicas. We use ONCV pseudopotentials[44,45] for all atoms along with a plane-wave kinetic energy cutoff of 80 Ry and a 3×3 $\mathbf{k}$-point Brillouin zone grid. The GW-BSE calculations are carried out with the Yambo code[37,38] using a 2D slab cutoff of the Coulomb interaction. For calculations of defects in monolayer hBN, a 3×3 $\mathbf{k}$-point grid is employed together with an energy cutoff of 10 Ry for the dielectric matrix. The number of empty bands included in the GW calculation (for the polarizability and self-energy summations) is 7 times the number of occupied bands. These parameters converge the exciton energy to within 0.1 eV in our test calculations on the $V_N N_B$ defect in a 4×4 supercell. For calculations on defects in bulk hBN, we use a 5×5×1 supercell containing two AA-stacked layers. The bulk case uses a 2×2×3 $\mathbf{k}$-point grid while all other parameters are the same as in the monolayer case.

Acknowledgement

Additional Information

Supplementary Information accompany this paper (at URL to be added).

Competing financial interests: The authors declare no competing financial interests.

References

(1) Liu, X.; Hersam, M. C. 2D materials for quantum information science. *Nat. Rev. Mater.* **2019**, *4*, 669–684.

(2) Chen, X.; Lu, X.; Dubey, S.; Yao, Q.; Liu, S.; Wang, X.; Xiong, Q.; Zhang, L.; Srivastava, A. Entanglement of single-photons and chiral phonons in atomically thin WSe$_2$. *Nat. Phys.* **2019**, *15*, 221–227.

(3) Tran, T. T.; Bray, K.; Ford, M. J.; Toth, M.; Aharonovich, I. Quantum emission from hexagonal boron nitride monolayers. *Nat. Nanotechnol.* **2016**, *11*, 37–41.

(4) Gottscholl, A.; Kianinia, M.; Soltamov, V.; Orlinskii, S.; Mamin, G.; Bradac, C.; Kasper, C.; Krambrock, K.; Sperlich, A.; Toth, M.; Aharonovich, I.; Dyakonov, V. Initialization and read-out of intrinsic spin defects in a van der Waals crystal at room temperature. *Nat. Mater.* **2020**, *19*, 540–545.

(5) Childress, L.; Gurudev Dutt, M. V.; Taylor, J. M.; Zibrov, A. S.; Jelezko, F.; Wrachtrup, J.; Hemmer, P. R.; Lukin, M. D. Coherent dynamics of coupled electron and nuclear spin qubits in diamond. *Science* **2006**, *314*, 281–285.

(6) Ladd, T. D.; Jelezko, F.; Laflamme, R.; Nakamura, Y.; Monroe, C.; O'Brien, J. L. Quantum computers. *Nature* **2010**, *464*, 45–53.

(7) Loophole-free Bell inequality violation using electron spins separated by 1.3 kilometres. *Nature* **2015**, *526*, 682–686.

(8) Aharonovich, I.; Englund, D.; Toth, M. Solid-state single-photon emitters. *Nat. Photonics* **2016**, *10*, 631–641.

(9) Caldwell, J. D.; Aharonovich, I.; Cassabois, G.; Edgar, J. H.; Gil, B.; Basov, D. N. Photonics with hexagonal boron nitride. *Nat. Rev. Mater.* **2019**, *4*, 552–567.

(10) Jungwirth, N. R.; Calderon, B.; Ji, Y.; Spencer, M. G.; Flatté, M. E.; Fuchs, G. D. Temperature dependence of wavelength selectable zero-phonon emission from single defects in hexagonal boron nitride. *Nano Lett.* **2016**, *16*, 6052–6057.

(11) Tran, T. T.; Elbadawi, C.; Totonjian, D.; Lobo, C. J.; Grosso, G.; Moon, H.; Englund, D. R.; Ford, M. J.; Aharonovich, I.; Toth, M. Robust multicolor single photon emission from point defects in hexagonal boron nitride. *2017 Conference on Lasers and Electro-Optics, CLEO 2017 - Proceedings* **2017**, *2017-Janua*, 1–2.

(12) Dietrich, A.; Bürk, M.; Steiger, E. S.; Antoniuk, L.; Tran, T. T.; Nguyen, M.; Aharonovich, I.; Jelezko, F.; Kubanek, A. Observation of Fourier transform limited lines in hexagonal boron nitride. *Phys. Rev. B* **2018**, *98*, 081414.

(13) Tawfik, S. A.; Ali, S.; Fronzi, M.; Kianinia, M.; Tran, T. T.; Stampfl, C.; Aharonovich, I.; Toth, M.; Ford, M. J. First-principles investigation of quantum emission from hBN defects. *Nanoscale* **2017**, *9*, 13575–13582.

(14) Weston, L.; Wickramaratne, D.; Mackoit, M.; Alkauskas, A.; Van de Walle, C. G. Native point defects and impurities in hexagonal boron nitride. *Phys. Rev. B* **2018**, *97*, 214104.

(15) Sajid, A.; Reimers, J. R.; Ford, M. J. Defect states in hexagonal boron nitride: Assignments of observed properties and prediction of properties relevant to quantum computation. *Phys. Rev. B* **2018**, *97*, 064101.

(16) López-Morales, G. I.; Proscia, N. V.; López, G. E.; Meriles, C. A.; Menon, V. M. Toward the identification of atomic defects in hexagonal boron nitride: X-ray photoelectron spectroscopy and first-principles calculations. *Preprint at arXiv:1811.05924*

(17) Noh, G.; Choi, D.; Kim, J. H.; Im, D. G.; Kim, Y. H.; Seo, H.; Lee, J. Stark tuning of single-photon emitters in hexagonal boron nitride. *Nano Lett.* **2018**, *18*, 4710–4715.

(18) Abdi, M.; Chou, J. P.; Gali, A.; Plenio, M. B. Color centers in hexagonal boron nitride monolayers: A group theory and ab initio analysis. *ACS Photonics* **2018**, *5*, 1967–1976.

(19) Turiansky, M. E.; Alkauskas, A.; Bassett, L. C.; Van De Walle, C. G. Dangling bonds in hexagonal boron nitride as single-photon emitters. *Phys. Rev. Lett.* **2019**, *123*, 127401.

(20) Bernardi, M.; Palummo, M.; Grossman, J. C. Extraordinary sunlight absorption and one nanometer thick photovoltaics using two-dimensional monolayer materials. *Nano Lett.* **2013**, *13*, 3664.

(21) Qiu, D. Y.; Da Jornada, F. H.; Louie, S. G. Optical spectrum of MoS_2: Many-body effects and diversity of exciton states. *Phys. Rev. Lett.* **2013**, *111*, 216085.

(22) Refaely-Abramson, S.; Qiu, D. Y.; Louie, S. G.; Neaton, J. B. Defect-induced modification of low-lying excitons and valley selectivity in monolayer transition metal dichalcogenides. *Phys. Rev. Lett.* **2018**, *121*, 167402.

(23) Attaccalite, C.; Bockstedte, M.; Marini, A.; Rubio, A.; Wirtz, L. Coupling of excitons and defect states in boron-nitride nanostructures. *Phys. Rev. B* **2011**, *83*, 144115.

(24) Rohlfing, M.; Louie, S. G. Electron-hole excitations and optical spectra from first principles. *Phys. Rev. B* **2000**, *62*, 4927.

(25) Palummo, M.; Bernardi, M.; Grossman, J. C. Exciton radiative lifetimes in two-dimensional transition metal dichalcogenides. *Nano Lett.* **2015**, *15*, 2794.

(26) Chen, H.-Y.; Palummo, M.; Sangalli, D.; Bernardi, M. Theory and ab initio computation of the anisotropic light emission in monolayer transition metal dichalcogenides. *Nano Lett.* **2018**, *18*, 3839.

(27) Chen, H.-Y.; Jhalani, V. A.; Palummo, M.; Bernardi, M. Ab initio calculations of exciton radiative lifetimes in bulk crystals, nanostructures, and molecules. *Phys. Rev. B* **2019**, *100*, 075135.

(28) Jhalani, V. A.; Chen, H.-Y.; Palummo, M.; Bernardi, M. Precise radiative lifetimes in bulk crystals from first principles: the case of wurtzite gallium nitride. *J. Phys.: Condens. Matter* **2019**, *32*, 084001.

(29) Loudon, R. *The Quantum Theory of Light*; OUP Oxford, 2000.

(30) Kimble, H. J.; Dagenais, M.; Mandel, L. Photon antibunching in resonance fluorescence. *Phys. Rev. Lett.* **1977**, *39*, 691.

(31) Giannozzi, P.; Baroni, S.; Bonini, N.; Calandra, M.; Car, R.; Cavazzoni, C.; Ceresoli, D.; Chiarotti, G. L.; Cococcioni, M.; Dabo, I.; et al., QUANTUM ESPRESSO: a modular and open-source software project for quantum simulations of materials. *J. Phys.: Condens. Matter.* **2009**, *21*, 395502.

(32) Hybertsen, M. S.; Louie, S. G. Electron correlation in semiconductors and insulators: Band gaps and quasiparticle energies. *Phys. Rev. B* **1986**, *34*, 5390.

(33) Exarhos, A. L.; Hopper, D. A.; Grote, R. R.; Alkauskas, A.; Bassett, L. C. Optical signatures of quantum emitters in suspended hexagonal boron nitride. *ACS Nano* **2017**, *11*, 3328–3336.

(34) Hayee, F.; Yu, L.; Zhang, J. L.; Ciccarino, C. J.; Nguyen, M.; Marshall, A. F.; Aharonovich, I.; Vučković, J.; Narang, P.; Heinz, T. F.; Dionne, J. A. Revealing multi-

ple classes of stable quantum emitters in hexagonal boron nitride with correlated optical and electron microscopy. *Nat. Mater.* **2020**, *19*, 534–539.

(35) Chejanovsky, N.; Rezai, M.; Paolucci, F.; Kim, Y.; Rendler, T.; Rouabeh, W.; Fávaro De Oliveira, F.; Herlinger, P.; Denisenko, A.; Yang, S.; Gerhardt, I.; Finkler, A.; Smet, J. H.; Wrachtrup, J. Structural attributes and photodynamics of visible spectrum quantum emitters in hexagonal boron nitride. *Nano Lett.* **2016**, *16*, 7037–7045.

(36) Choi, S.; Tran, T. T.; Elbadawi, C.; Lobo, C.; Wang, X.; Juodkazis, S.; Seniutinas, G.; Toth, M.; Aharonovich, I. Engineering and localization of quantum emitters in large hexagonal boron nitride layers. *ACS Appl. Mater. Interfaces* **2016**, *8*, 29642–29648.

(37) Marini, A.; Hogan, C.; Grüning, M.; Varsano, D. Yambo: An ab initio tool for excited state calculations. *Comput. Phys. Commun.* **2009**, *180*, 1392–1403.

(38) Sangalli, D. et al. Many-body perturbation theory calculations using the yambo code. *J. Phys.: Condens. Matter* **2019**, *31*, 325902.

(39) Cudazzo, P.; Tokatly, I. V.; Rubio, A. Dielectric screening in two-dimensional insulators: Implications for excitonic and impurity states in graphane. *Phys. Rev. B* **2011**, *84*, 085406.

(40) Andersen, K.; Latini, S.; Thygesen, K. S. Dielectric genome of van der Waals heterostructures. *Nano Lett.* **2015**, *15*, 4616–4621.

(41) Von Toussaint, U. Bayesian inference in physics. *Rev. Mod. Phys.* **2011**, *83*, 943–999.

(42) Li, S.; Chou, J.-P.; Hu, A.; Plenio, M. B.; Udvarhelyi, P.; Thiering, G.; Abdi, M.; Gali, A. Giant shift upon strain on the fluorescence spectrum of $V_N N_B$ color centers in h-BN. *Preprint at arXiv:2001.02749*

(43) Perdew, J. P.; Burke, K.; Ernzerhof, M. Generalized gradient approximation made simple. *Phys. Rev. Lett.* **1996**, *77*, 3865.

(44) Hamann, D. R. Optimized norm-conserving Vanderbilt pseudopotentials. *Phys. Rev. B* **2013**, *88*, 085117.

(45) Schlipf, M.; Gygi, F. Optimization algorithm for the generation of ONCV pseudopotentials. *Comput. Phys. Commun.* **2015**, *196*, 36–44.